Supplementary Discussion

Copy-number and structural variations within the FOXA1 locus
To validate the structural variation (SV) calls, we carried out whole-genome sequencing (WGS) of four index cases and identified a matched genomic breakpoint in all of them (**Extended Data Fig. 1l and Supplementary Table 2**). We also called copy-number breakends based on whole-exome sequencing (WES) of 370 metastatic samples and copy-number variant (CNV) analysis (**Supplementary Table 3**). Bearing in mind that only a subset of genomic rearrangements results in CNVs or fusions, we detected a highly significant overlap between the two readouts (odds-ratio=6.81, p=4.3e-09; **Extended Data Fig. 1m**). WGS of three additional cases with copy-number breakends again confirmed a precise genomic breakpoint (**Extended Data Fig. 1l**). Because of inherent limitation in the sensitivity of WGS, RNA-seq and CNVs for the detection of SVs, we estimate the recurrence of FOXA1 locus rearrangements at 20%-30% in mCRPC (**Extended Data Fig. 1n**). For FOXA1 mutations, all the cases were heterozygous and the gene itself showed copy-number gains in over 50% of the cases, without a single event of homozygous deletion (**Extended Data Fig. 2a,b**).

FOXA1 expression in mCRPC
We assessed the expression of FOXA1 in different clinical stages of PCa, notably controlling for the variation in percent tumor content of primary and metastatic PCa across patient specimens. Here, we found a stage-wise increasing trend in the mRNA expression of FOXA1 (**Extended Data Fig. 2c**). This is consistent with parallel protein-level increase described in multiple immunohistochemical studies[55-57]. Together, this genomic alteration profile strongly suggests FOXA1 to be an oncogene in AR-dependent PCa.

Single particle tracking (SPT) and cistromic characterization of FOXA1 class1 mutants
Fundamental biophysical studies have revealed that transcription factors (TFs) search for their specific binding sites by random scanning of the genome[58-60]. In this model, rapid diffusion through nuclear space and transient binding with chromatin are primary determinants of TF scanning efficiency[6]. Thus, we assessed the chromatin interaction dynamics of class1 mutants in live cells using the single particle tracking technique. As previously described[61], based on the rate of diffusion, Halo-tagged fluorescent FOXA1 particles were classified into slow, fast or unbound fractions. Corroborating the FRAP data, distinct class1 mutants displayed a striking increase in nuclear diffusion with 3-4 fold reduction in the slow fraction relative to the WT protein (**Extended Data Fig. 3h,i**). This was accompanied with a parallel increase in the fast and/or unbound fractions of class1 mutants. Interestingly, the average chromatin dwell time of the fast diffusing fraction was 6-10 times smaller than the slow fraction (**Extended Data Fig. 3h**). Furthermore, class1 mutants generally had shorter dwell times on chromatin than WT FOXA1, suggesting that class1 mutants interact with the chromatin more dynamically than WT FOXA1.

Next, we thoroughly characterized the class1 mutant cistrome and assessed its impact on chromatin binding of AR. We performed FOXA1 and AR ChIP-seq experiments in 22RV1 cells with overexpression of either WT or class1 variants (I176M or R261G). Interestingly, the

class1 cistrome entirely overlapped with the WT FOXA1 binding sites (**Extended Data Fig. 3l,m**). *De novo* and supervised motif analyses further confirmed the consensus FOXA1 motif as the most significantly enriched motif in the two cistromes (**Extended Data Fig. 3o-q**). Further, in both cistromes, we found a similar enrichment of *de novo* motifs of known FOXA1 cofactors, such as NFI and HOXB13 (**Extended Data Fig. 3o**). Using known TF motifs, we found a comparable enrichment of AR and AR cofactor motifs between the WT and the mutant cistrome (**Extended Data Fig. 3o,r**). Consistently, both WT and class1 AR cistromes majorly overlapped with matched FOXA1 binding sites (**Extended Data Fig. 3n**). Additionally, the WT and class1 FOXA1 sites had comparable genomic distribution and were found predominantly within intergenic and intronic regions (**Extended Data Fig. 3s**). Thus, the DNA sequence-specificity, cistromic footprint and localization, and cofactor enrichment profile of class1 mutants are very similar to those of WT FOXA1. Together, these results suggest that the highly mobile class1 mutants are more efficient in scanning for, and engaging with, their genomic targets than WT FOXA1. In other words, we posit that class1 mutants can more frequently interact with AR-activated enhancers than WT FOXA1, and thereby induce a higher transcriptional response from these regulatory elements. Notably, this model is consistent with the previously described inductive role for pioneering TFs[62-64].

Cistromic characterization of FOXA1 class2 mutants

We thoroughly characterized the augmented class2 cistrome using the isogenic CRISPR-engineered PCa models. From the overlap analyses of the N-terminal cistromes, we defined three subsets of FOXA1 binding sites: WT-specific, common, and mutant-specific, using the simple overlap and the read fold-change strategies (**Extended Data Fig. 7a**). Notably, *de novo* and supervised motif analyses revealed the consensus FOXA1 motif as the most significantly enriched motif in all the three subsets (**Extended Data Fig.7a-c**). This suggests that class2 mutants also recognize the consensus FOXA1 motif. Intriguingly, cofactor enrichment analyses revealed the class2-specific sites to be markedly depleted of AR and AR cofactors motifs (**Extended Data Fig. 7d,e**). However, these motifs were comparably enriched in the common binding sites and the WT-specific sites (**Extended Data Fig. 7a,d,e**). The class2-specific sites instead were enriched for the CTCF motif and a higher fraction of these sites was within intronic and intergenic regions that are enriched for enhancer elements (**Extended Data Fig. 7e,f**). Together, this data suggests that class2 mutants retain binding at functionally essential AR sites (i.e. the common sites), and acquire binding at novel regulatory sites that are enriched for other TFs, such as CTCF.

Molecular mechanism of WNT activation in class2-mutant PCa

To uncover the underlying molecular mechanism of aberrant WNT activation in class2 mutant tumors, we referred to published FOXA1 protein interactome datasets[57,65] and looked for bonafide co-repressors that bind to the C-terminal domain of FOXA1. The TLE family of proteins emerged as notable interactors that bind to the Engrailed Homology 1 motif (400-408 amino acids) in FOXA1[66-68], and reportedly repress the LEF/TCF transcriptional complex[69,70]. Thus, we set out to explore the functional interplay between FOXA1 and TLE genes in PCa cells.

In AR/FOXA1 positive PCa cells, only TLE3 was considerably expressed (>1 FPKM; **Extended Data Fig. 8a**). Interestingly, knockdown experiments in PCa cells revealed TLE3 to be transcriptionally activated by FOXA1, but not AR (**Extended Data Fig. 8b)**, with a strong binding of FOXA1 within the early intronic region of TLE3 (**Extended Data Fig. 8c**). As TLE3 co-repressors do not have a personal DNA-binding domain[71], we performed ChIP-seq experiments to identify its chromatin tethering partner in PCa cells. Remarkably, in LNCaP and C42B cells, TLE3 cistromes almost entirely (>90%) overlapped with the WT FOXA1 binding sites (**Extended Data Fig. 8d**). Additionally, *de novo* motif analysis returned FOXA as the most significantly enriched motif in the TLE3 cistrome (bottom, **Extended Data Fig. 8d**). This raised a pertinent question: how is chromatin recruitment of TLE3 affected in the presence of the C-terminal truncated class2 mutants? To address this, we first used co-immunoprecipitation assays to confirm that WT and class1 mutant variants interacted with TLE3, while three distinct FOXA1 class2 mutants had lost this interaction (**Extended Data Fig. 8e**). Next, we repeated TLE3 ChIP-seq in isogenic WT and class2 mutant CRISPR clones, all of which had a comparable expression of TLE3. Again, TLE3 entirely co-localized with FOXA1 in the WT clones (**Fig.3g**). Remarkably, however, in class2 mutant clones, chromatin binding of TLE3 was markedly diminished (**Fig. 3h and Extended Data Fig. 8f-h**). This implies that the cistromically-dominant class2 mutants dislodge TLE3 (along with WT FOXA1) from the chromatin, and thereby transcriptionally disable repressive functions of TLE3. We functionally mimicked TLE3 chromatin-untethering via siRNA knockdown and performed RNA-Seq. Inactivation of TLE3 led to a significant up-regulation of WNT and EMT pathway genes (**Extended Data Fig. 8i**), including canonical WNT targets, such as LEF1, TCF4 and AXIN2 (**Extended Data Fig. 8j**). Notably, this is consistent with upregulation of LEF1 in the mutant clones (**Extended Data Fig. 7j**), and the motif-based prediction of LEF/TCF complex being the putative driver of class2 upregulated genes (**Extended Data Fig. 7h**). We also *de novo* discovered the LEF/TCF motif in the class2-specific cistrome (**Extended Data Fig. 7a**). Most remarkably, transcriptomic analyses revealed the genes up-regulated in 22RV1 cells upon TLE3 knockdown to be significantly enriched for class2 up-regulated genes (**Extended Data Fig. 8k**). Altogether, these data suggest that TLE3 binding to the chromatin is largely dependent on the C-terminal domain of FOXA1 and that the truncated, cistromically-dominant class2 mutants effectively abrogate TLE3-mediated repression of WNT-signaling in PCa cells.

The FAST, FURIOUS, and LOUD aberrations of FOXA1

By leveraging an aggregate PCa cohort of over 1500 cases, we were able to identify three previously undescribed structural classes of FOXA1 aberrations that diverged in genetic associations and oncogenic gain-of-functions. Hence, we establish FOXA1 as a potent oncogene that is altered by activating genetic aberrations in AR-dependent PCa. Overall, FOXA1 aberrations are observed in 34.6% of mCRPC (**Fig. 1h**). Class1 mutants, recurrent at approximately 9%, originate in primary PCa that lack other primary driver alterations[72]. Contrarily, class2 mutants recur at 4% and are clonally found only in metastatic PCa. Finally, class3 genomic rearrangements are significantly enriched in the metastatic disease and, within the limitations of RNA-seq and WES, are observed in 20-30% of cases. Notably, class1 and class2 alterations are entirely mutually exclusive, while class3 tandem-duplications frequently

co-occur with class2 mutations (odds-ratio=3.95, p=0.014). Furthermore, FOXA1 alterations are mainly found in AR-positive PCa, with limited or no recurrence reported in NE tumors[73].

Class1 FOXA1 mutations disrupt the Wing2 secondary structure and increase the transactivational ability of FOXA1 towards oncogenic AR-signaling (**Fig. 2h**). In contrast, class2 aberrations truncate the C-terminus and impart cistromic dominance to potentiate WNT/β-Catenin signaling that promotes metastasis *in vivo* (**Fig. 3i**). This also attributes a unique role to the C-terminal domain of FOXA1 in hindering its interaction with chromatin. We demonstrate both class1 and class2 mutations to be neomorphic (i.e., result in a novel gain-of-function). Class3 rearrangements fall into two structural patterns: translocations that place putative oncogenes in the proximity of the FOXMIND enhancer, and duplications that preserve and amplify the FOXMIND-FOXA1 regulatory domain (**Fig. 4e**). Class3 rearrangements provide a mechanism to increase FOXA1 expression to supraphysiological levels.

Recent sequencing studies have uncovered activating alterations in FOXA1 regulatory regions in estrogen receptor (ER)-positive breast cancer, including hotspot mutations in the FOXA1 promoter[74] and cancer-predisposing SNPs at FOXA1 binding sites[75,76]. Here, we show that the FOXA1 locus is structurally rearranged in breast cancer as well. FOXA1 mutations are also observed in bladder cancer and AR-positive salivary gland tumors[77]. Thus, the three classes of FOXA1 alterations might be distinctly activating in other tumors with oncogenic AR or ER signaling. However, further experimentation is required to elucidate their disease-specific functions and clinical correlations.

In summary, our study presents genetic, mechanistic and phenotypic evidence supporting FOXA1 mutations as activating driver alterations in AR-driven PCa (**Supplementary Table 4**), and likely in other hormone-receptor driven cancers. Additionally, for the first time, we describe structural rearrangement as an important mechanism of FOXA1 pathogenic activation and delineate FOXMIND as a critical enhancer element recurrently altered in PCa. The high prevalence of FOXA1 alterations (about 35%), further emphasizes that mCRPC is a disease of aberrant TF activity, already exemplified by both ETS fusions and AR alterations present in over half of mCRPC[78]. Considering the strong oncogenic effects of FOXA1 alterations demonstrated in this study, co-targeting FOXA1 is an attractive therapeutic approach for mCRPC as well as other FOXA1-driven cancers.

Supplementary Discussion References:

55. Jain, R. K., Mehta, R. J., Nakshatri, H., Idrees, M. T. & Badve, S. S. High-level expression of forkhead-box protein A1 in metastatic prostate cancer. *Histopathology* **58**, 766–772 (2011).
56. Gerhardt, J. *et al.* FOXA1 promotes tumor progression in prostate cancer and represents a novel hallmark of castration-resistant prostate cancer. *Am. J. Pathol.* **180**, 848–861 (2012).
57. Robinson, J. L. L. *et al.* Elevated levels of FOXA1 facilitate androgen receptor chromatin binding resulting in a CRPC-like phenotype. *Oncogene* **33**, 5666–5674 (2014).
58. Misteli, T. Protein dynamics: implications for nuclear architecture and gene expression. *Science* **291**, 843–847 (2001).
59. Phair, R. D. *et al.* Global nature of dynamic protein-chromatin interactions in vivo: three-dimensional genome scanning and dynamic interaction networks of chromatin proteins. *Mol. Cell. Biol.* **24**, 6393–6402 (2004).
60. Hager, G. L., McNally, J. G. & Misteli, T. Transcription dynamics. *Mol. Cell* **35**, 741–753 (2009).
61. Swinstead, E. E. *et al.* Steroid Receptors Reprogram FoxA1 Occupancy through Dynamic Chromatin Transitions. *Cell* **165**, 593–605 (2016).
62. Carroll, J. S. *et al.* Chromosome-wide mapping of estrogen receptor binding reveals long-range regulation requiring the forkhead protein FoxA1. *Cell* **122**, 33–43 (2005).
63. Zaret, K. S. & Carroll, J. S. Pioneer transcription factors: establishing competence for gene expression. *Genes Dev.* **25**, 2227–2241 (2011).
64. Iwafuchi-Doi, M. *et al.* The Pioneer Transcription Factor FoxA Maintains an Accessible Nucleosome Configuration at Enhancers for Tissue-Specific Gene Activation. *Mol. Cell* **62**, 79–91 (2016).
65. Jozwik, K. M., Chernukhin, I., Serandour, A. A., Nagarajan, S. & Carroll, J. S. FOXA1 Directs H3K4 Monomethylation at Enhancers via Recruitment of the Methyltransferase MLL3. *Cell Rep.* **17**, 2715–2723 (2016).
66. Wang, J. C. *et al.* Transducin-like enhancer of split proteins, the human homologs of Drosophila groucho, interact with hepatic nuclear factor 3beta. *J. Biol. Chem.* **275**, 18418–18423 (2000).
67. Copley, R. R. The EH1 motif in metazoan transcription factors. *BMC Genomics* **6**, 169 (2005).
68. Sekiya, T. & Zaret, K. S. Repression by Groucho/TLE/Grg proteins: genomic site recruitment generates compacted chromatin in vitro and impairs activator binding in vivo. *Mol. Cell* **28**, 291–303 (2007).
69. Cavallo, R. A. *et al.* Drosophila Tcf and Groucho interact to repress Wingless signalling activity. *Nature* **395**, 604–608 (1998).
70. Daniels, D. L. & Weis, W. I. Beta-catenin directly displaces Groucho/TLE repressors from Tcf/Lef in Wnt-mediated transcription activation. *Nat. Struct. Mol. Biol.* **12**, 364–371 (2005).
71. Chen, G. & Courey, A. J. Groucho/TLE family proteins and transcriptional repression. *Gene* **249**, 1–16 (2000).
72. Cancer Genome Atlas Research Network. The Molecular Taxonomy of Primary Prostate Cancer. *Cell* **163**, 1011–1025 (2015).
73. Beltran, H. *et al.* Divergent clonal evolution of castration-resistant neuroendocrine prostate cancer. *Nat. Med.* **22**, 298–305 (2016).
74. Rheinbay, E. *et al.* Recurrent and functional regulatory mutations in breast cancer. *Nature* **547**, 55 (2017).
75. Cowper-Sal lari, R. *et al.* Breast cancer risk-associated SNPs modulate the affinity of

chromatin for FOXA1 and alter gene expression. *Nat. Genet.* **44**, 1191–1198 (2012).
76. Zhang, X., Cowper-Sal lari, R., Bailey, S. D., Moore, J. H. & Lupien, M. Integrative functional genomics identifies an enhancer looping to the SOX9 gene disrupted by the 17q24.3 prostate cancer risk locus. *Genome Res.* **22**, 1437–1446 (2012).
77. Dalin, M. G. *et al.* Comprehensive Molecular Characterization of Salivary Duct Carcinoma Reveals Actionable Targets and Similarity to Apocrine Breast Cancer. *Clin. Cancer Res.* **22**, 4623–4633 (2016).
78. Robinson, D. *et al.* Integrative clinical genomics of advanced prostate cancer. *Cell* **161**, 1215–1228 (2015).

Supplementary Table 2 | Summary of structural variants in the FOXA1 locus from DNA and RNA sequencing.

Tumor ID	5' Chr DNA	5' position DNA	3' Chr DNA	3' position DNA	5' Chr RNA	5' position RNA	3' Chr RNA	3' position RNA	Label
WA57	chr14	37558144	chr14	61443099	chr14	37556368	chr14	61391289	BND
WA57	chr2	105296350	chr14	37558176	chr2	105296355	chr14	37558175	BND
WA46	chr14	35828813	chr14	37722358	chr14	35831409	chr14	37714797	DUP
MO1584	chr14	39040137	chr14	39673330	chr14	39040731	chr14	39668554	DUP
MO1637	chr14	36867647	chr14	41556096					BND
WA37	chr14	37512779	chr6	110894981					BND
WA37	chr14	37232151	chr14	37583694	chr14	37247102	chr14	37564363	DUP
SC9221	chr14	37176305	chr14	37477340					DUP
SC9221	chr14	36030634	chr14	37590665					DUP
MO1788	chr14	35320494	chr14	37590028					DUP

Structural variants were called in 7 cases subject to whole-genome sequencing, a subset of transcribed junctions were also detected by RNA-seq. Label: BND - breakend not otherwise specified, DUP - duplication.

Supplementary Table 3 | Summary of copy-number breakends from whole-exome sequencing data.

Tumor ID	Chr	Breakend mid-point	Breakend interval
MO_1118	chr14	37210290	37172750-37247830
MO_1118	chr14	37546323	37545829-37546818
MO_1232	chr14	37674042	37595022-37753063
MO_1232	chr14	38025742	37842419-38209066
MO_1234	chr14	37461485	37423047-37499923
MO_1234	chr14	37593797	37592744-37594850
MO_1553	chr14	37396256	37369656-37422857
MO_1553	chr14	37674042	37595022-37753063
MO_1788	chr14	37591250	37591223-37591277
MO_1901	chr14	36844464	36814054-36874875
MO_1901	chr14	37210290	37172750-37247830
MO_1901	chr14	37546323	37545829-37546818
MO_1901	chr14	37808099	37807469-37808730
MO_1995	chr14	37674042	37595022-37753063
MO_1995	chr14	38025742	37842419-38209066
SC_9001	chr14	37789201	37787722-37790681
SC_9001	chr14	37839836	37837521-37842152
SC_9009	chr14	37257430	37248023-37266837
SC_9009	chr14	37591250	37591223-37591277
SC_9012	chr14	37800774	37796940-37804609
SC_9017	chr14	37691380	37595022-37787738
SC_9038	chr14	37546323	37545829-37546818
SC_9062	chr14	37674042	37595022-37753063
SC_9062	chr14	37800774	37796940-37804609
SC_9068	chr14	37691380	37595022-37787738
SC_9084	chr14	37787730	37787722-37787738
SC_9086	chr14	37800774	37796940-37804609
SC_9089	chr14	37023700	36875092-37172308
SC_9089	chr14	37546323	37545829-37546818
SC_9093	chr14	37534664	37523687-37545642
SC_9093	chr14	37674042	37595022-37753063
SC_9103	chr14	37789205	37787740-37790670
SC_9123	chr14	37546323	37545829-37546818
SC_9132	chr14	38025742	37842419-38209066
SC_9140	chr14	37461485	37423047-37499923
SC_9140	chr14	37674042	37595022-37753063
SC_9140	chr14	37805583	37804826-37806340
SC_9140	chr14	38025742	37842419-38209066
SC_9175	chr14	37546323	37545829-37546818
SC_9200	chr14	37787730	37787722-37787738
SC_9211	chr14	36684692	36684658-36684727
SC_9211	chr14	37787730	37787722-37787738
SC_9215	chr14	37787730	37787722-37787738
SC_9218	chr14	37338985	37308531-37369439
SC_9218	chr14	37511825	37500178-37523473
SC_9221	chr14	37210290	37172750-37247830
SC_9221	chr14	37461485	37423047-37499923
SC_9221	chr14	37569199	37547121-37591277

SC_9221	chr14	38025742	37842419-38209066
SC_9224	chr14	37674042	37595022-37753063
SC_9227	chr14	37062394	36952480-37172308
SU2C_06115122	chr14	37396256	37369656-37422857
SU2C_06115233	chr14	37523498	37500178-37546818
SU2C_06115233	chr14	37695640	37595022-37796258
SU2C_06115242	chr14	38025742	37842419-38209066
TP_2078	chr14	37674042	37595022-37753063
TP_2078	chr14	37789196	37787722-37790670
TP_2249	chr14	36913691	36875092-36952290
TP_2249	chr14	37534664	37523687-37545642
WA_07	chr14	37023662	36875071-37172254
WA_07	chr14	37257350	37247958-37266742
WA_12	chr14	37023647	36875040-37172254
WA_12	chr14	37674027	37594997-37753058
WA_14	chr14	36662803	36662789-36662818
WA_14	chr14	37787705	37787673-37787738
WA_24	chr14	36255049	35775610-36734489
WA_24	chr14	37810580	37808847-37812313
WA_28	chr14	37266898	37266864-37266932
WA_33	chr14	37674027	37594997-37753058
WA_46	chr14	38025859	37842343-38209376
WA_55	chr14	37569167	37546998-37591336
WA_55	chr14	37695637	37594997-37796278
WA_56	chr14	37810551	37808850-37812252

Copy number breakends were identified from segmented log(tumor/normal) coverage ratios and mirrored B-allele frequencies. The Breakend interval represents the genomic interval containing the inferred genomic breakpoint i.e. it is the interval between adjacent exons assigned to different copy-number segments. The mid-point represents the center of this interval used for plotting.

Supplementary Table 4 | Class-specific summary of primary features of FOXA1 alterations in advanced prostate cancer.

Alteration class	Alteration type	Structural impact	Clinical recurrence		Clonality	Genetic co-alterations	Functional impact
			primary PCa	mCRPC			
Class 1 ('FAST')	Coding mutations (enriched for missense and inframe indels) within the DNA-binding forkhead domain of FOXA1 (168-269aa), clustered at the C-terminal end.	Alter or disrupt the Wing2 secondary structure of the forkhead domain	8-9%	8-9%	Heterozygous clonal	1) Depleted for ETS-fusions, SPOP-mutations, and PI3K pathway alterations. 2) Enriched for DNA repair deficient, mismatch repair deficient, and WNT pathway alterations. 3) No association to AR or AR pathway alterations.	1) Mutations impart faster nuclear mobility and increased chromatin sampling frequency. 2) Class1 mutants are stronger trans-activators of AR-signaling.
Class 2 ('FURIOUS')	Coding mutations (enriched for frameshifting indels) in the C-terminal end of FOXA1, after the forkhead domain.	Truncate or disrupt the C-terminal regulatory domain of FOXA1, which includes the Engrailed Homology 1 motif (400-408aa)	1%	3-4%	Subclonal in primary PCa; heterozygous clonal in mCRPC	1) Enriched for RB1 deletions in mCRPC. 2) No association to AR or AR pathway alterations.	1) Mutations impart higher binding affinity to the FOXA1 DNA element. 2) Class2 mutants are cistromically-dominant and displace WT FOXA1 and TLE3 from the chromatin to activate WNT signaling.
Class 3 ('LOUD')	Structural rearrangements (enriched for tandem duplications) within the FOXA1 genetic locus	Reposition (in case of tlocs) or duplicate (in case of tandem dups) a conserved FOXA1 enhancer element, which we annotated as FOXMIND.	8-9%	20-30%	NA	Enriched for FOXA1 Class2 alterations.	1) Repositioning of FOXMIND drives overexpression of putative oncogenes (including ETV1, MYC, SKIL) that translocate into the FOXA1 locus. 2) Duplication of FOXMIND drives overexpression of FOXA1 itself.

Structural, clinical, genetic and functional features of the three classes of FOXA1 alterations are summarized. PCa, prostate cancer; mCRPC, metastatic castration-resistant prostate cancer; FOXMIND, FOXA1 mastermind.

Supplementary Figure 1

Note: For all experiments, when probing for proteins with different molecular weights, membranes were pre-cut around the expected molecular sizes with 20KDa margins on either side. When probing for proteins with similar molecular weights, duplicate membranes were used and a control protein (e.g. GAPDH, BActin, Vinculin, Total H3) was probed on each.

Extended Data Fig. 1c

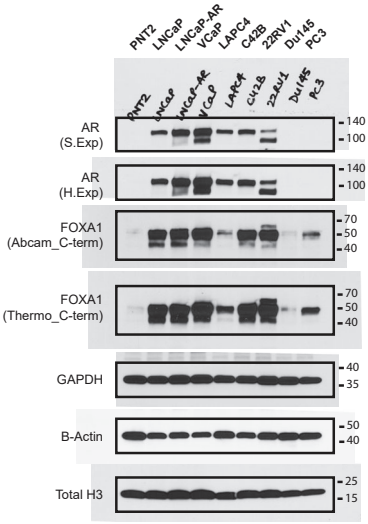

Extended Data Fig. 1d and e

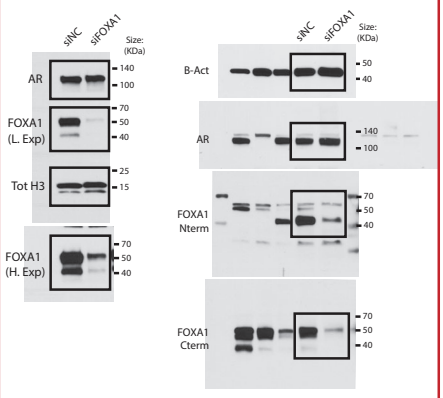

Extended Data Fig. 4a

Extended Data Fig. 5b

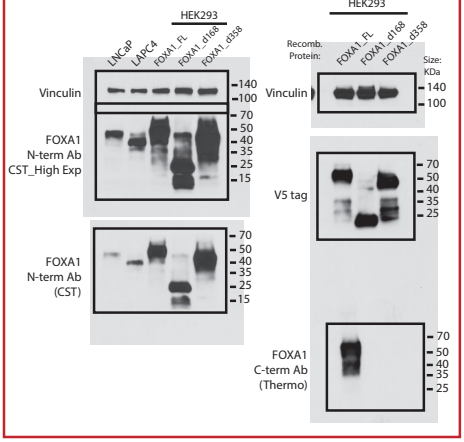

Extended Data Fig. 4b

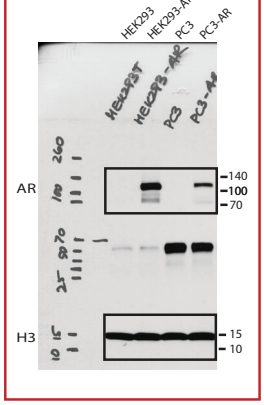

Extended Data Fig. 4c

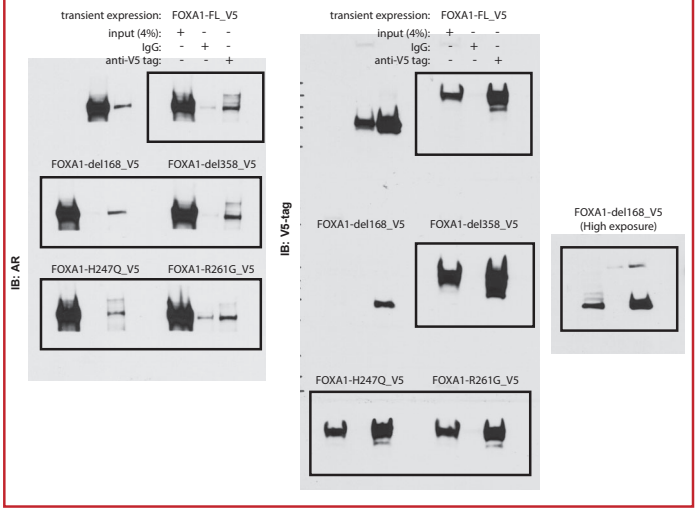

Extended Data Fig. 4e

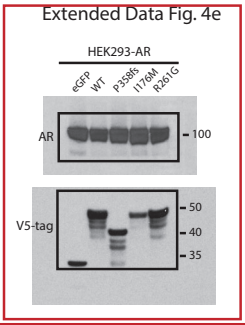

Extended Data Fig. 4d

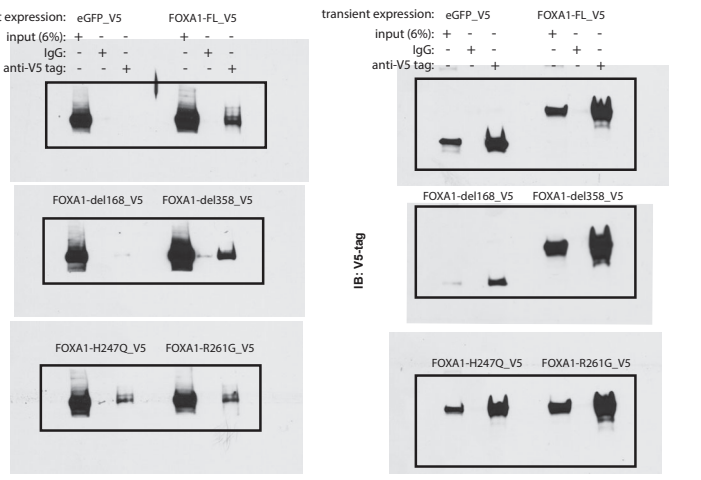

Extended Data Fig. 5d

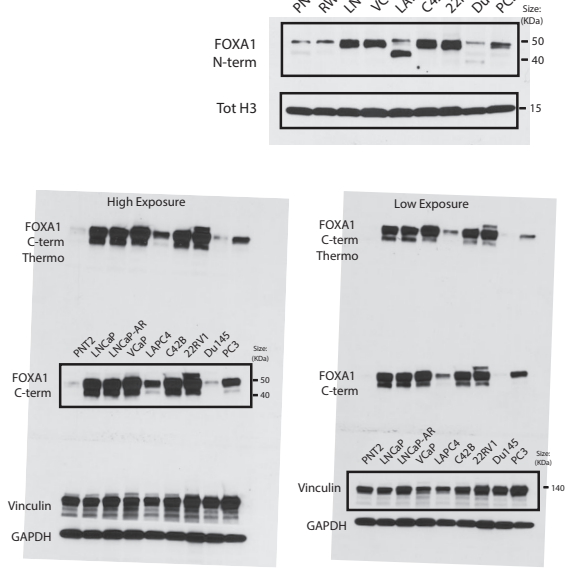

Note: These immunoblots were run alongside the blots in Extended Data Fig. 1b

Extended Data Fig. 5e

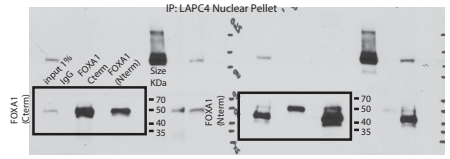

Extended Data Fig. 5f

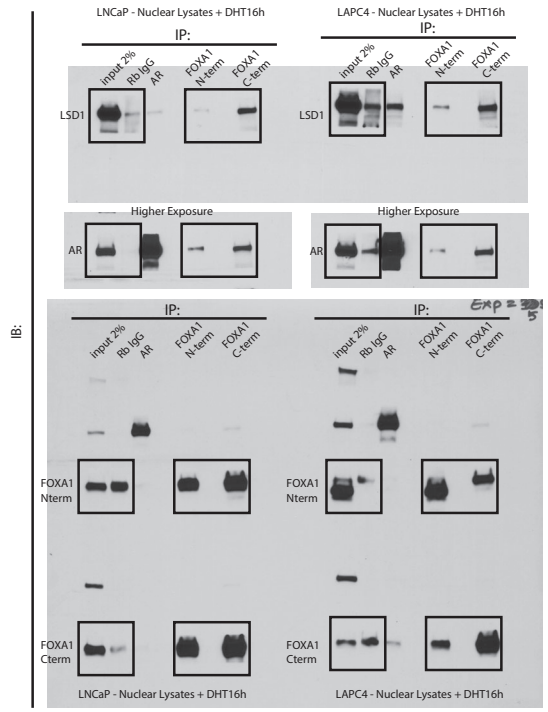

Fig. 3c

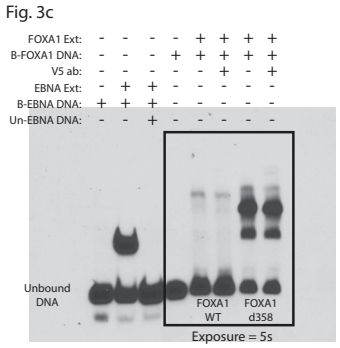

Extended Data Fig. 6b

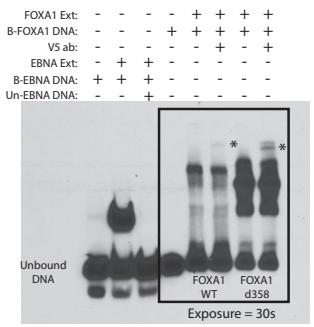

Extended Data Fig. 6d

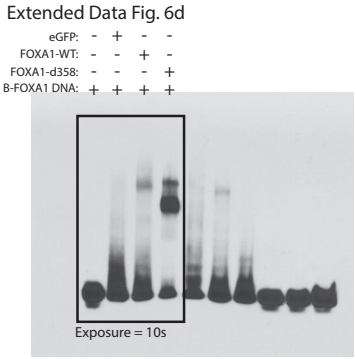

Extended Data Fig. 6c

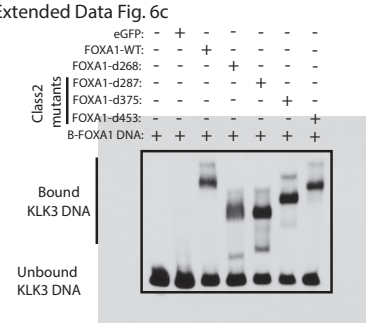

Extended Data Fig. 6a

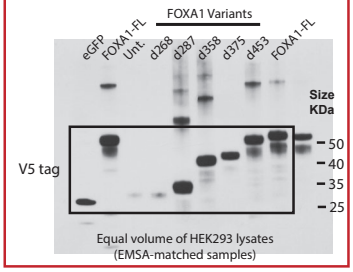

Extended Data Fig. 7i

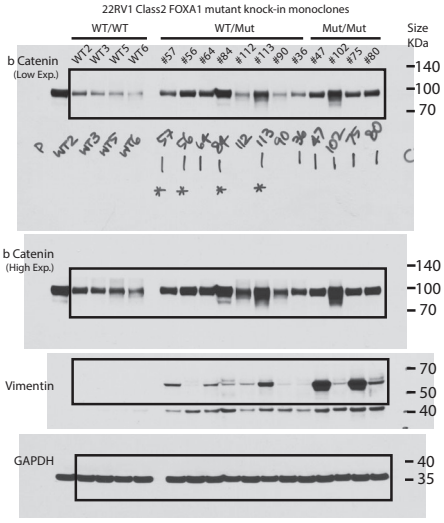

Extended Data Fig. 6g

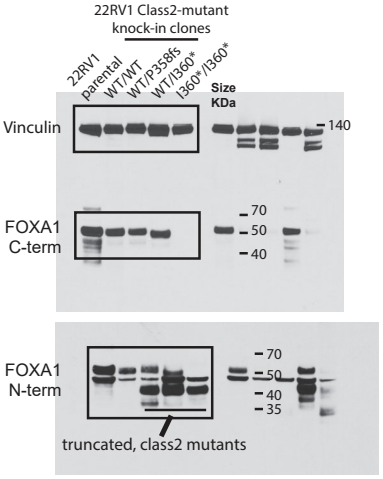

Extended Data Fig. 7j

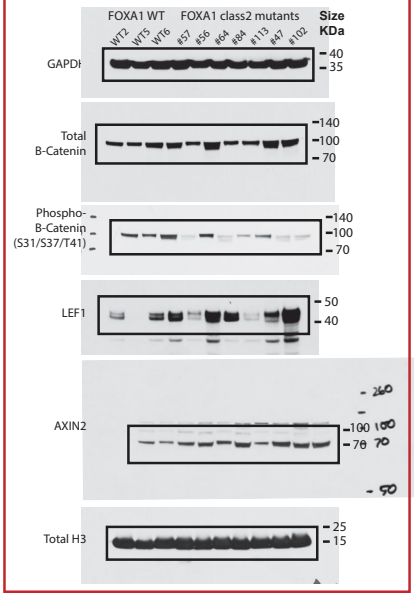

Extended Data Fig. 8a

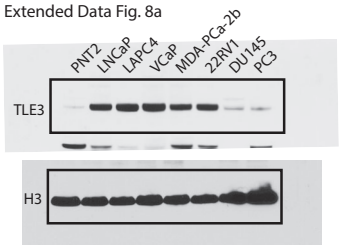

Extended Data Fig. 6h

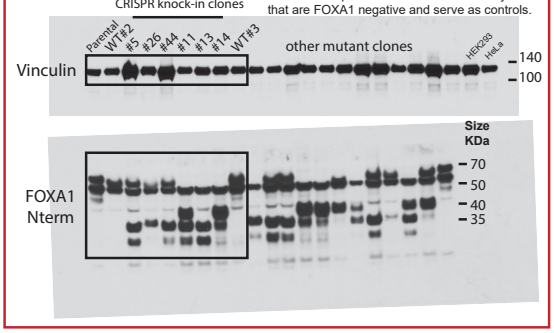

Extended Data Fig. 8b

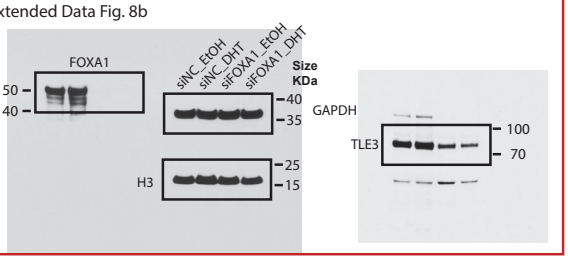

Extended Data Fig. 8e

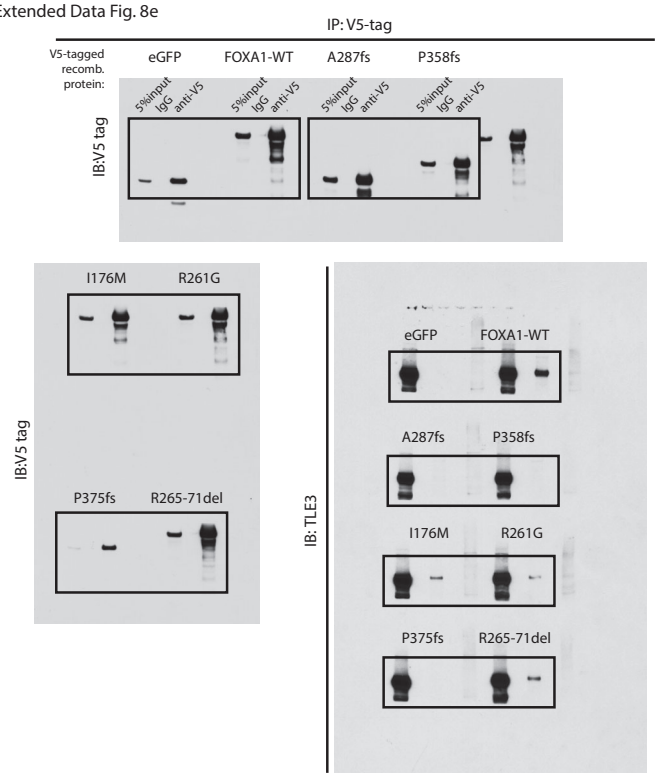

Extended Data Fig. 8j